Face-gear drive: Simulation of shaping as manufacturing process of face-gears

Author(s):
Zschippang, H. Andreas; Weikert, Sascha; Wegener, Konrad

Publication date:
2022-06

Permanent link:
https://doi.org/10.3929/ethz-b-000536822

Originally published in:
Mechanism and Machine Theory 172, https://doi.org/10.1016/j.mechmachtheory.2022.104791

Mechanism and Machine Theory 172 (2022) 104791

Contents lists available at ScienceDirect

Mechanism and Machine Theory

journal homepage: www.elsevier.com/locate/mechmt

Research paper

Face-gear drive: Simulation of shaping as manufacturing process of face-gears

H. Andreas Zschippang [a,*], Sascha Weikert [a], Konrad Wegener [b]

[a] Inspire AG, Zürich, Switzerland
[b] Institute of Machine Tools and Manufacturing, ETH Zürich, Switzerland

ARTICLE INFO

Keywords:
Face-gear
Gear shaping simulation
Cutting force calculation
Cutting force measurement
Tool wear

ABSTRACT

Gear shaping is the most important process for manufacturing internal gears. Even if this method is also suitable for the production of spur gears, these can be produced more effectively using hobbing. Gear shaping is also interesting for manufacturing of face-gears. Since the shaper cutter is quite simple compared to a hob and the tool costs are therefore relatively low, this method is particularly suitable for small series production. This manuscript deals with the simulation of gear shaping of face-gears with the aim of determining suitable process parameters such as radial and rotary infeed and thus achieving a stable manufacturing process as fast as possible and with low reject rate. The cutting forces are determined on the basis of the theoretical uncut chip thickness, whereby the tool deflection can be calculated using these, provided that the stiffness of the tool, machine tool and component holder is known. In addition, the tool wear can be estimated using a suitable wear model. Experimentally determined cutting forces during the shaping of a face-gear are used to validate the simulation model.

1. Introduction

The most important processes for manufacturing of face gears are hobbing and shaping. A patent for a hob for producing face gears was published by Miller [1] in 1942. A hob for a face-gear is a comparatively complex tool that cannot be used flexibly. The hob for a cylindrical gear is based on a reference rack profile, which means that the helix angle and profile shift of the workpiece can be varied as required. In contrast, the hob for the production of face-gears is based on the shaper and is therefore a comparatively complex tool that cannot be used flexibly. This hob is practically only suitable for face-gears which are based on the same shaper geometry. In addition, these tools are custom-made, which is why hobbing for the production of small quantities is uneconomical. The company Crown Gear B.V. (NL) has patents from 1992 [2] and 1994 [3] relating to the geometry of hob cutters for the production of spur face-gears; another patent [4] from 1994 relates to a hob for producing helical face-gears. Wang et al. [5] examined the geometry generation of hob cutters for manufacturing of face gears and manufactured some gears and then measured them. Furthermore, Wang et al. [6] developed an assembly hob and examined it experimentally.

Gear shaping is not as effective as manufacturing using a hob, but the required tool is far less complex and therefore cheaper to obtain. Although gear shaping is mentioned in many publications, detailed studies of this process in relation to manufacturing of face-gears are rare. Shen and Tong [7] have dealt with the shaping of face gears and investigated this experimentally. The gear shaping of spur and ring gears has been researched much more intensely. Erkorkmaz et al. [8] developed a new model to predict the uncut chip geometry and cutting forces in shaping. Katz et al. [9–11] intensified the research and expanded the model to take

* Corresponding author.
E-mail address: zschippang@inspire.ethz.ch (H.A. Zschippang).

https://doi.org/10.1016/j.mechmachtheory.2022.104791
Received 29 October 2021; Received in revised form 14 February 2022; Accepted 18 February 2022
Available online 11 March 2022

into account tool deflection, elastic deformations and virtual gear metrology. Xu et al. [12] investigated the gear shaping of a gear rack with a variable gear ratio. The focus was on the simulation of gear shaping and the calculation of the cutting forces.

In this manuscript, a method for the simulation of the gear shaping of face-gears is described. The resulting cutting forces, tool deflection and tool wear are calculated. The experimentally determined cutting forces during shaping of a face-gear show that the simulated forces agree well with the measured values.

Nomenclature

α_{sc}	Tip clearance angle of shaper cutter
$\bar{\mu}$	Mean friction coefficient
$\bar{T}_{chip}$	Mean temperature
β	Helix angle
β_a	Averaged friction angle
β_n	Friction angle
β_{TQ}	Taylor–Quinney coefficient
Δx_d, Δy_d, Δz_d	Displacement due to tool deflection
η_c	Chip flow angle
γ	Shaft angle
ϕ_{sn}	Shear angle of the primary deformation zone
γ_n	Rake angle
γ_{sc}	Tip rake angle of shaper cutter
λ_s	Inclination angle
ω_2	Rotational speed of face-gear
ω_{st}	Rotational speed of cutting stroke
ϕ_2	Angle of rotation of the face-gear
ϕ_c	Angle of rotation of the shaper cutter
γ_1	Shear strain at the outflow of the primary shear band
ρ_m	Density
σ_t	Normal stress along the rake face
σ_{t_0}	Normal stress at the cutting edge
τ_0	Shear stress at the entry of the primary shear band
τ_s	Shear stress in the primary deformation zone
$\underline{\underline{M}}_{2c_d}(t)$	Transformation matrix to transform the shaper cutter from its own coordinate system (system rotating with the shaper cutter) to the face-gear coordinate system (system rotating with the face-gear) taking tool deflection into account
$\underline{\underline{M}}_{2c}(t)$	Transformation matrix to transform the shaper cutter from its own coordinate system (system rotating with the shaper cutter) to the face-gear coordinate system (system rotating with the face-gear)
$\underline{F}$	Total force vector
F_c, F_f, F_p	Cutting, feed and passive force
$\underline{n}_i^*$	Mean normal direction
$\underline{r}_{c/c0}$	Position vector of cutting edge
$\underline{r}_{c2}$	Position vector of cutting edge in face-gear coordinate system S_2
ξ_d	Profile parameter
a_r	Mean radial infeed
a_{acc}	Acceleration of radial infeed
a_{circ}	Circumferential infeed
$a_{r_{end}}$	Radial infeed at end position of the shaper cutter
$a_{r_{start}}$	Radial infeed at start position of the shaper cutter
b	Chip width
c	Specific heat capacity
C_1, C_2	Wear characteristic constants for Usui formula
d_r	Radial position of the shaper cutter
$d_{r_{end}}$	Radial end position of the shaper cutter
$d_{r_{start}}$	Radial starting position of the shaper cutter

dL	Sliding distance
dt	Time increment
dW	Wear rate
E	Axle offset
$\underline{F}_{c_i}, \underline{F}_{f_i}, \underline{F}_{p_i}$	Cutting, feed and passive force vector
F_s	Shear force
F_{c_e}, F_{f_e}	Edge force component of cutting and feed force
F_{c_s}, F_{f_s}	Shear component of cutting and feed force
f_{st}	Cutting stroke frequency
h	Uncut chip thickness
H_2	Tooth height of the face-gear
h_c	Measured chip thickness
h_{max}	Maximum uncut chip thickness
k	Thermal conductivity
k_x, k_y	Stiffness
K_γ	Cutting force correction factor considering the rake angle
$k_{c1,1}, k_{f1,1}, k_{p1,1}$	Specific cutting, feed and passive force
K_{c_e}, K_{f_e}	Specific cutting an feed force due to rubbing or ploughing at the tool cutting edge
K_{c_s}, K_{f_s}	Specific cutting and feed force due to shearing at the shear zone and friction at the rake face
K_c	Cutting force correction factor in cutting direction
K_f	Cutting force correction factor in feed direction
K_{sp}	Cutting force correction factor considering chip compression
K_{v_c}	Cutting force correction factor considering the cutting speed
K_{wear}	Cutting force correction factor considering the tool wear
l	Distance to the tool tip
l_2^*	Distance to the face-gear axis
l_c	Position of the shaper cutter
$l_{c_{top}}$	Upper stoke position of the shaper cutter
L_{crank}	Length of the driven crank
l_{ct}	Chip-tool contact length
l_{st}	Stroke length of the shaper cutter
l_{top}	Top overrun length of the shaper cutter
m_c, m_f, m_p	Kienzle exponent for cutting, feed and passive force
m_{2c}	Gear ratio between the shaper cutter and the face-gear
N_2	Number of teeth of the face-gear
N_c	Number of teeth of the shaper cutter
p_c	Pitch radius of shaper cutter
r_c	Pitch radius of the shaper cutter
r_{comp}	Chip compression ratio
t	Time
t_r	Time required for the radial movement from the start to the end position
T_w	Absolute temperature of the work-piece
T_{chip_1}	Temperature at the outflow of the primary shear band
T_{chip}	Temperature of the chip surface
v	Cutting speed
v_c	Chip velocity
$v_{r_{end}}$	Speed at which the shaper cutter is moved radially at end position
$v_{r_{start}}$	Speed at which the shaper cutter is moved radially at start position

2. Process kinematics

The kinematics of gear shaping is the superposition of three different movement components: the double stroke movement of the tool, the rotary feed movements of the tool and workpiece, which are proportional to the transmission ratio, and the radial

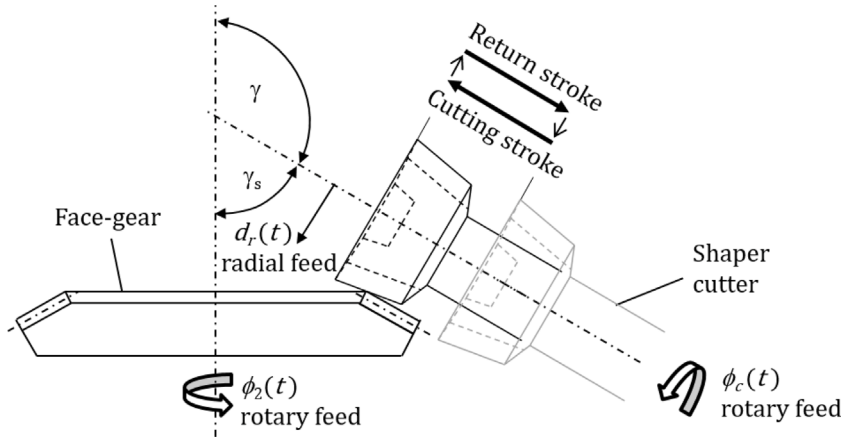

Fig. 1. Gear shaping of a face-gear: Geometry and kinematics.

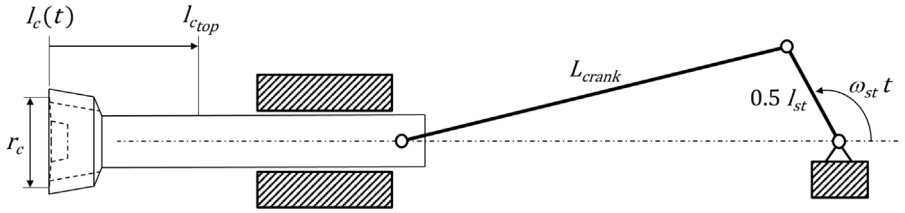

Fig. 2. Schematic view of a slider crank mechanism.

feed movement. During the cutting stroke, the chip removal takes place from the outside into the workpiece. The return stroke is carried out with a tool offset to prevent the tool from rubbing against the workpiece. This process is shown schematically in Fig. 1. Theoretically, all variants of face gears can be produced by means of gear shaping, i.e. with any shaft angle, axle offset and helix angle. Limitations come more from the structure and the number of axes of the machine tool as well as the maximum possible stroke length.

The stroke movement of the shaper cutter can be described using the slider crank equation

$$l_c(t) = l_{c_{top}} - \frac{l_{st}}{2}(1-\cos(\omega_{st}t)) + \sqrt{L_{crank}^2 - \frac{l_{st}^2}{4}\sin^2(\omega_{st}t)} - L_{crank} \tag{1}$$

where l_c is the position of the shaper cutter, $l_{c_{top}}$ is the upper stoke position of the shaper cutter, l_{st} is the stroke length (distance of the upper to the lower stroke position), L_{crank} is the length of the driven crank and ω_{st} is the cutting stroke angular velocity. The slider crank mechanism is shown schematically in Fig. 2.

If the length of the crank is much larger than the stroke length, Eq. (1) simplifies to

$$l_c(t) = l_{c_{top}} - \frac{l_{st}}{2}(1-\cos(\omega_{st}t)) \tag{2}$$

An investigation by Katz [11] shows that the simplification is permissible for modern gear shaping machines and that the deviations from the exact equation are minimal. The cutting stroke angular velocity ω_{st} can be calculated by

$$\omega_{st} = 2\,\pi\,f_{st} \tag{3}$$

where f_{st} is the cutting stroke frequency.

The rotary feed is defined by a circumferential infeed a_{circ} on the pitch circle of the cutter per double stroke. Regarding the angular velocity of the face-gear follows

$$\omega_2 = a_{circ}\frac{f_{st}\,m_{2c}}{r_c} \tag{4}$$

where r_c is the pitch radius of the shaper cutter and m_{2c} is the gear ratio between the shaper cutter and the face-gear

$$m_{2c} = \frac{N_c}{N_2} \tag{5}$$

N_c is the number of teeth of the shaper cutter and N_2 is the number of teeth of the face-gear. For the angle of rotation of the face-gear over time it thus follows

$$\phi_2(t) = \omega_2 \, t \tag{6}$$

The angle of rotation of the shaper cutter ϕ_c is coupled to the angle of rotation of the face-gear ϕ_2 via the transmission ratio. However, if a helical face-gear is to be cut, the shaper cutter must be rotated synchronously with the double stroke movement according to the helix angle. Thus, for the angle of rotation ϕ_c of the shaper cutter follows

$$\phi_c(t) = \frac{\omega_2 \, t}{m_{2c}} + l_c(t) \, p \tag{7}$$

where the pitch p is linked to the helix angle β and is determined by

$$p = \frac{\tan \beta}{r_c} \tag{8}$$

The radial feed takes place along the tooth height of the face-gear, starting from the tooth tip to the tooth root. The radial feed thus refers to the shaper cutter. However, the tooth root is only ideal as the end point. Usually, after the first gear has been manufactured, the flanks are measured and the maximum immersion depth is adjusted according to the shape deviations and the resulting tooth thickness. There is also the option of implementing a small offset between the shaper cutter and the face-gear if corrections to the symmetry of the teeth are necessary. Such fine adjustments are especially of great advantage after regrinding the shaper cutter. Assuming that the radial infeed d_r is zero at the position where the tooth tip of the face-gear touches the addendum diameter of the shaper cutter, $d_{r_{start}}$ is the starting position of the shaper cutter and $d_{r_{end}}$ is the end position of the radial infeed. Thus $d_{r_{start}}$ must be less than or equal to zero. The radial infeed can be varied depending on the gear shaping machine and its control. It is common to reduce the radial infeed over the submerged depth in order to counteract an increase in the machining forces. In the event that the acceleration of the radial infeed is to be constant, the time-dependent radial position $d_r(t)$ of the shaper cutter can be calculated simply based on two given infeeds $a_{r_{start}}$ and $a_{r_{end}}$ at the radial start and end position. The speeds at which the shaper cutter is moved radially at the start and end position are thus

$$v_{r_{start}} = a_{r_{start}} \, f_{st} \tag{9}$$

and

$$v_{r_{end}} = a_{r_{end}} \, f_{st} \tag{10}$$

From the equation of motion of an uniformly accelerated movement, one obtains the time t_r which is required for the radial movement from the start to the end position and the acceleration a_{acc}

$$t_r = \frac{2(d_{r_{end}} - d_{r_{start}})}{v_{r_{start}} + v_{r_{end}}} \tag{11}$$

$$a_{acc} = \frac{v_{r_{end}} - v_{r_{start}}}{t_r} \tag{12}$$

The mean radial infeed a_r is therefore

$$a_r = \frac{a_{r_{start}} + a_{r_{end}}}{2} \tag{13}$$

For the time-dependent radial position d_r of the shaper cutter it follows

$$d_r(t) = \begin{cases} \frac{a_{acc}}{2} t^2 + v_{r_{start}} \, t + d_{r_{start}}, & t < t_r \\ d_{r_{end}}, & t \geq t_r \end{cases} \tag{14}$$

3. Calculation of undeformed chip geometry

In order to calculate the material removal and the theoretical uncut chip thickness along the tool cutting edge, the tool engagement with the workpiece is calculated for each cutting stroke. In this way, the face-gear tooth geometry is calculated stroke by stroke. The differences between the individual geometries between two cutting strokes thus correspond to the material removal per cutting stroke, from which in turn the undeformed chip geometry can be derived. For this purpose, the tool cutting edge is first discretized. It does not matter whether the end face of the shaper cutter is conical or, as in the case of shaper cutters for the production of helical gears, each individual tooth is set at a helix angle. The individual points $\underline{r}_{c0}$ should simply correspond to the exact contour of the tool. To simulate gear shaping, the tool is first shifted in its own tool coordinate system according to the stroke position. The following applies to every single point on the tool cutting edge

$$\underline{r}_c(t) = \underline{r}_{c0} + \begin{bmatrix} 0 \\ 0 \\ l_c(t) \end{bmatrix} \tag{15}$$

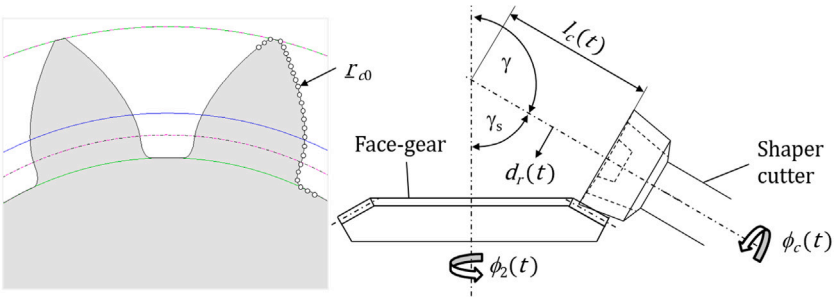

Fig. 3. Left: Discretization of the too cutting edge; right: Shifting the tool according to the stroke position.

The discretization of the cutting edge and the shift of the tool according to the stroke position are shown schematically in Fig. 3.

In the next step, the tool geometry and also kinematics are transformed into the coordinate system of the face-gear, taking into account the individual infeeds. The corresponding transformation matrix $\underline{\underline{M}}_{2c}$ also takes into account the time-dependent position of the shaper cutter. Here, γ is the shaft angle, E is the axle offset and H_2 is the tooth height of the face-gear. The transformation matrix is given by

$$\underline{\underline{M}}_{2c}(t) = \begin{bmatrix} \cos\phi_c\cos\phi_2 + \sin\phi_c\sin\phi_2\cos\gamma & -\sin\phi_c\cos\phi_2 + \cos\phi_c\sin\phi_2\cos\gamma & -\sin\phi_2\sin\gamma & -E\cos\phi_2 \\ -\cos\phi_c\sin\phi_2 + \sin\phi_c\cos\phi_2\cos\gamma & \sin\phi_c\sin\phi_2 + \cos\phi_c\cos\phi_2\cos\gamma & -\cos\phi_2\sin\gamma & E\sin\phi_2 \\ \sin\phi_c\sin\gamma & \cos\phi_c\sin\gamma & \cos\gamma & \frac{H_2 - d_r(t)}{\sin\gamma} \\ 0 & 0 & 0 & 1 \end{bmatrix} \tag{16}$$

with

$$\begin{aligned} \phi_c &= \phi_c(t) \\ \phi_2 &= \phi_2(t) \end{aligned} \tag{17}$$

For a single point $\underline{r}_c$ on the cutting edge of the tool, the corresponding point $\underline{r}_{c2}$ in the face-gear coordinate system S_2 is given by

$$\begin{aligned} \underline{r}_{c2}(t) &= \underline{\underline{M}}_{2c}(t)\underline{r}_c^*(t) \\ \text{with } \underline{r}_c^*(t) &= \begin{bmatrix} r_{c_x}(t) \\ r_{c_y}(t) \\ r_{c_z}(t) \\ 1 \end{bmatrix} \end{aligned} \tag{18}$$

In order to keep the gear shaping simulation as efficient as possible, to keep the computing time to a minimum, the face-gear is discretized across the tooth flank length. For a shaft angle of $\gamma = 90°$, there are therefore cutting lines of the tooth geometries on cylinder surfaces, for a shaft angle of $\gamma \neq 90°$ there are therefore cutting lines on individual cones. The unmachined face-gear thus consists at the beginning of a number of points building circular lines in the individual sections, which represent the tooth tip. In the following, the individual sections are cut with the contour of the shaper cutter for a cutting stroke. To calculate the correct intersection points, the time t must be determined iteratively for each individual point $\underline{r}_{c2}(t)$ on the cutting edge until it lies on the respective cylinder or cone. The equation to be fulfilled is thus

$$l_2^* = \begin{cases} \sqrt{r_{c2_x}(t)^2 + r_{c2_y}(t)^2}, & \gamma = 90° \\ \cos\gamma\left(r_{c2_z}(t) + \tan\gamma\sqrt{r_{c2_x}(t)^2 + r_{c2_y}(t)^2}\right), & \gamma \neq 90° \end{cases} \tag{19}$$

where l_2^* is the given distance to the face-gear axis for a section. The points of intersection between the tool and the resulting face-gear can now be determined in the coordinate system of the cylinders or cones. The geometries of the face-gear and tool are approximated for this in a simplified manner by connecting the individual points using straight lines. The contour of the face-gear is replaced with the contour of the shaper cutter between the two points of intersection between the tool and the face-gear. The respective difference thus corresponds to the material removal, i.e. the undeformed chip.

The uncut chip thickness for a point on the tooth cutting edge $\underline{r}_{c2}(t)$ is determined in the direction of its normal vector. If the theoretical chip removal is now calculated from cutting stroke to cutting stroke, the face-gear tooth geometry develops with increasing time t. Fig. 4 shows the simulation of the chip removal for the gear shaping of a face-gear for a selected cutting stroke.

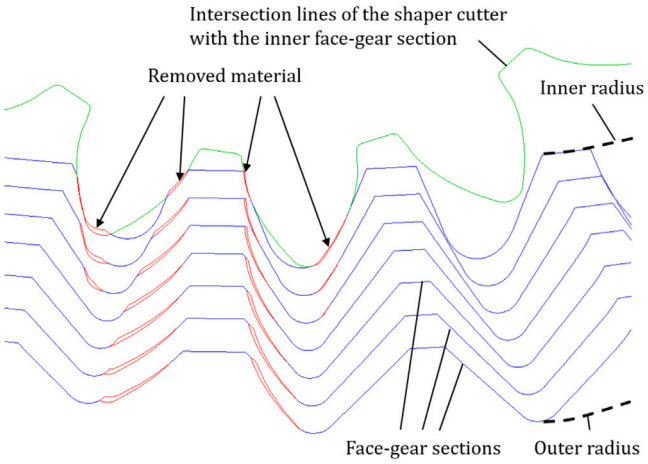

Fig. 4. Simulation of the chip removal for the gear shaping of a face-gear for a selected cutting stroke. The theoretical material removal is determined for a given number of sections across the tooth width.

4. Cutting forces

The Kienzle equation [13] is ideally suited for estimating the cutting forces in orthogonal cutting. The general form of the Kienzle equation is as follows

$$\begin{aligned} F_c &= k_{c1,1}\, h^{1-m_c}\, b\, K_c \\ F_f &= k_{f1,1}\, h^{1-m_f}\, b\, K_f \\ F_p &= k_{p1,1}\, h^{1-m_p}\, b\, K_p \end{aligned} \tag{20}$$

where F_c is the cutting force in cutting direction, F_f in the feed direction and F_p is the passive force component orthogonal to both other forces. The corresponding specific forces $k_{c1,1}$, $k_{f1,1}$ and $k_{p1,1}$ relate to a chip cross-section of a chip width of $b = 1$ mm and an uncut chip thickness of $h = 1$ mm. The exponents m_c, m_f and m_p describe the slope of the curves. The Kienzle parameters are usually determined experimentally by lathing attempts in orthogonal cutting. K_c, K_f and K_p are corresponding correction factors to take into account parameters that differ from the experiments. The correction factors have been steadily expanded over the years to take into account, for example, the influence of tool wear, the tool material, the cutting speed, the rake angle and others. However, an application of this equation is made more difficult if it is no longer an orthogonal cut. Either the parameters of the Kienzle equation were determined with a corresponding angle of inclination, or an extended model is required to estimate the cutting forces. Yazar et al. [14] refer, for example, to experimental investigations by König [15] and their extensions of the Kienzle equation in order to take into account the influence of the tool inclination angle. However, the availability of the data for many materials is limited.

Another possibility is to use a model proposed by Budak et al. [16] or Altintas [17] to transform orthogonal to oblique cutting. Kaymakci et al. [18] builds on this, for example, a unified cutting force model for turning, boring, drilling and milling operations. Erkorkmaz et al. [8] and Katz et al. [9–11] follow this strategy to estimate the cutting forces for gear shaping.

So the cutting forces can be determined using the Kienzle equation for the orthogonal cut. The passive force is zero for the orthogonal cut, which means that only the cutting force F_c and feed force F_f are calculated. All corrections due to the rake angle, cutting speed, tool wear, etc. are taken into account. This is followed by the transformation of the cutting forces for the orthogonal cut to oblique cut depending on the local inclination of the tool cutting edge. The calculation steps required for this are based on the publications by Budak et al. [16] and Altintas [17] and are briefly explained below. The relevant angles and the forces for oblique cutting are shown in Fig. 5

The cutting force F_c and the feed force F_f can each be divided into a shear component (F_{c_s}, F_{f_s}) and an edge force component (F_{c_e}, F_{f_e})

$$\begin{aligned} F_c &= F_{c_s} + F_{c_e} = K_{c_s}\, h\, b + K_{c_e}\, b \\ F_f &= F_{f_s} + F_{f_e} = K_{f_s}\, h\, b + K_{c_e}\, b \\ F_p &= 0 \end{aligned} \tag{21}$$

where K_{c_s} and K_{f_s} are the specific cutting forces due to shearing at the shear zone and friction at the rake face in relation to the chip cross-sectional area; K_{c_e} and K_{f_e} are the edge forces per unit width of the cutting edge due to rubbing or ploughing [17]. The edge forces can be estimated approximately by extrapolating the measured forces for an uncut chip thickness to $h = 0$. The Kienzle equation itself is unsuitable for this, since the forces are also zero with an uncut chip thickness of $h = 0$. Since the tip rake angle of the shaper cutters is rather small, the differences in the forces from the orthogonal cut, converted to oblique cut, are rather small,

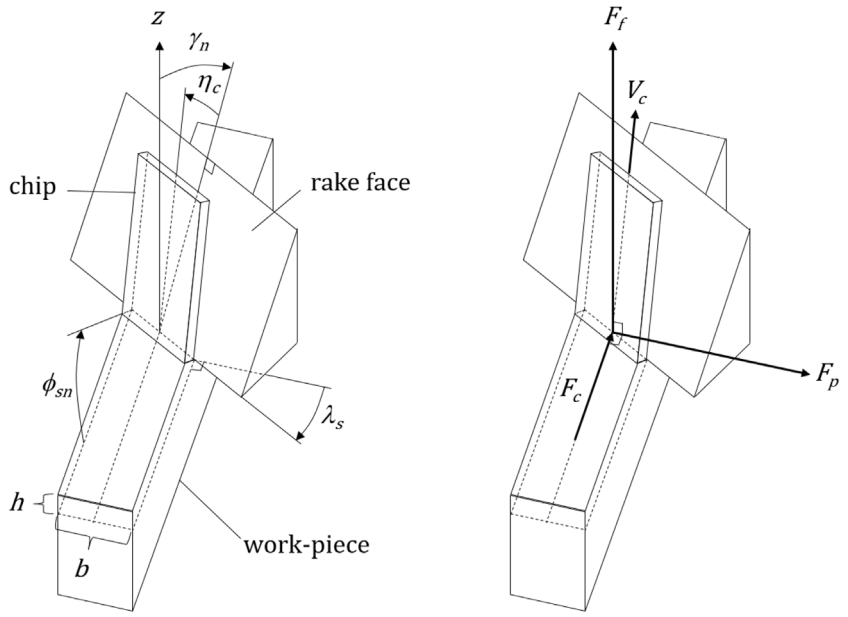

Fig. 5. Forces and angles for oblique cutting.
Source: Adapted from Altintas [17].

so that, for the sake of simplicity, the cutting force F_c and the feed force F_f are equated with the respective shear component. The shear force F_s can be determined from the shear force components in the cutting and feed directions

$$F_s = F_{c_s} \cos \phi_{sn} - F_{f_s} \sin \phi_{sn} \tag{22}$$

where ϕ_{sn} is the shear angle of the primary deformation zone. For the shear stress τ_s in the primary deformation zone follows

$$\tau_s = \frac{F_s \sin \phi_{sn}}{bh} \tag{23}$$

The shear angle ϕ_{sn} can be determined experimentally by measuring the chip thickness h_c and the uncut chip thickness h. The following applies:

$$\tan \phi_{sn} = \frac{r_{comp} \cos \gamma_n}{1 - r_{comp} \cos \gamma_n}, \text{ with } r_{comp} = \frac{h}{h_c} \tag{24}$$

where r_{comp} is the chip compression ratio and γ_n is the rake angle. However, it is time-consuming to run tests first to measure the chips and data on the shear angle are often missing in the literature for some materials. The shear angle can therefore be estimated using the formula by Lee and Shaffer [19]

$$\phi_{sn} = \frac{\pi}{4} + \gamma_n - \beta_a \tag{25}$$

It is a fairly simple but workable formula. The solution of the shear angle ϕ_{sn} depends only on the rake angle γ_n and the averaged friction angle β_a. Kovrizhnykh [20] compared the results with experiments and came up with good matches. However, this equation can be expanded to improve the results [20]. In this case, the original Lee and Shaffer formula is used. The averaged friction angle β_a for orthogonal cutting is calculated by

$$\beta_a = \gamma_n + \arctan \frac{F_{f_s}}{F_{c_s}} \tag{26}$$

The edge forces in relation to the chip width K_{c_e} and K_{f_e} as calculated for the orthogonal cut, can be taken over to oblique cutting. The situation with the cutting forces due to shear in the shear zone and friction on the rake face in relation to the cross-sectional area of the chip is different. According to Altintas [17] and Armarego [21] the cutting forces for oblique cutting can be calculated

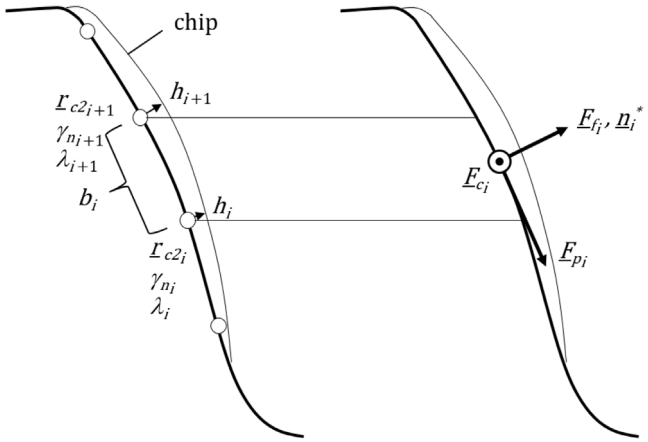

Fig. 6. Schematic representation of the discretization of the cutting edge and the necessary geometric parameters to determine the individual cutting forces. The distances between the points along the cutting edge are much smaller in practical use.

by

$$\begin{aligned} F_c &= \frac{\tau_s b h}{\sin\phi_{sn}} \cdot \frac{\cos(\beta_n - \gamma_n) + \tan\lambda_s \tan\eta_c \sin\beta_n}{\sqrt{\cos^2(\phi_{sn} + \beta_n - \gamma_n) + \tan^2\eta_c \sin^2\beta_n}} + K_{c_e} \cos\lambda_s b \\ F_f &= \frac{\tau_s b h}{\sin\phi_{sn}\cos\lambda_s} \cdot \frac{\sin(\beta_n - \gamma_n)}{\sqrt{\cos^2(\phi_{sn} + \beta_n - \gamma_n) + \tan^2\eta_c \sin^2\beta_n}} + K_{f_e} b \\ F_p &= \frac{\tau_s b h}{\sin\phi_{sn}} \cdot \frac{\cos(\beta_n - \gamma_n)\tan\lambda_s - \tan\eta_c \sin\beta_n}{\sqrt{\cos^2(\phi_{sn} + \beta_n - \gamma_n) + \tan^2\eta_c \sin^2\beta_n}} + K_{c_e} \sin\lambda_s b \end{aligned} \tag{27}$$

where λ_s is the inclination angle and η_c is the chip flow angle. The friction angle β_n is calculated by

$$\tan\beta_n = \tan\beta_a \cos\eta_c \tag{28}$$

The shear stress τ_s, the normal shear angle ϕ_{sn} and the average friction angle β_a are determined for the orthogonal cut and are assumed to be identical for oblique cutting. As an approximation, it can be assumed that the angle of inclination λ_s and the chip flow angle η_c are identical, which may be approximately correct at least for small angles of inclination. For more precise calculations, the formula by Armarego [21] can be used to estimate the chip flow angle η_c. This formula describes the relationship between the individual angles for classical oblique cutting:

$$\tan(\beta_n + \phi_{sn}) = \frac{\tan\lambda_s \cos\gamma_n}{\tan\eta_c - \sin\gamma_n \tan\lambda_s} \tag{29}$$

To calculate the cutting forces when shaping face-gears, the cutting edge is discretized, as shown in Fig. 3. The cutting edge is thus divided into N edge elements based on the individual points on the cutting edge $\underline{r}_{c2_i}$, and the forces are calculated for each element. It is assumed that the various elements do not affect each other, since the changes in uncut chip thickness from element to element are small. It is assumed that slightly larger gradients in uncut chip thickness across the cutting edge, which occur in a tapered manner, are negligible when determining the total force acting on the tool. The normal rake angle γ_{n_i}, the angle of inclination λ_i, the uncut chip thickness h_i and the current cutting speed v_{c_i} are determined for each individual point $\underline{r}_{c2_i}(t)$. The uncut chip thickness h_i is determined in each case based on the previously calculated uncut chip thicknesses in the face-gear sections. For this purpose, the distance to the face-gear axis l_2 is determined for the point $\underline{r}_{c2_i}(t)$ according to Eq. (19). The uncut chip thickness h_i is calculated using the corresponding uncut chip thicknesses in the adjacent face-gear sections defined by l_2^* by linear interpolation over the distance. For the calculation of the individual cutting forces, two adjacent points $\underline{r}_{c2_i}$ and $\underline{r}_{c2_{i+1}}$ on the cutting edge are taken into account. Thus, all parameters are averaged over the adjacent points. The chip width b_i is the distance between two adjacent points. The cutting force $\underline{F}_{c_i}$ points into the cutting direction, the feed force $\underline{F}_{f_i}$ points into the mean normal direction $\underline{n}_i^*$ and the passive force $\underline{F}_{p_i}$ is orthogonal to both other forces. To obtain the total forces acting on the tool, the individual cutting forces are summed up over the entire tool cutting edge. The discretization of the cutting edge and the necessary geometric parameters to determine the individual cutting forces are shown in Fig. 6.

The total force that acts on the tool is thus

$$\underline{F} = \sum_{i=0}^{N-1} \underline{F}_{c_i} + \underline{F}_{f_i} + \underline{F}_{p_i} \tag{30}$$

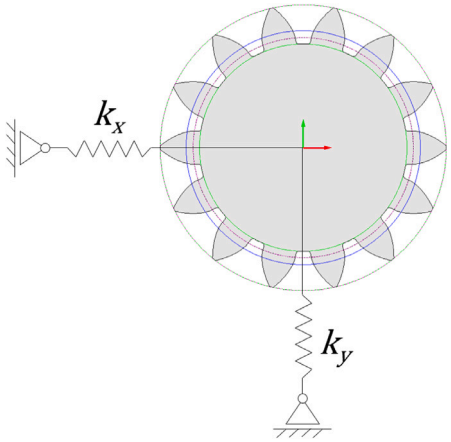

Fig. 7. Substitute model to take into account the stiffnesses determined orthogonal to the stroke direction to determine the tool deflection.

5. Tool deflection

In order to take the tool deflection into account, the rigidity of the shaping machine tool, the shaper cutter and the workpiece clamping must be known. It is often difficult to calculate these stiffnesses, since the internal structure and dimensions of the machine tool are usually not known in detail. The experimental determination of the total stiffness is therefore much simpler. Measurement of the stiffness using piezo sensors is ideal for this purpose. Such a sensor is mounted on the workpiece clamp in place of the workpiece in accordance with the direction of the stiffness to be measured. Then, instead of a shaper cutter, a cylindrical tool with similar dimensions is moved to the piezo sensor using the machine axis in small steps in the measuring direction and the resulting force curve is recorded at the same time. The resulting force divided by the infeed thus corresponds to the stiffness of the overall system in the measured direction, with all relevant components being automatically included in the result except for the stiffness of the workpiece itself.

The relevant directions with regard to the tool deflection are those orthogonal to the stroke direction. Since the stroke direction in the tool coordinate system is the z-direction, the stiffnesses must be determined in the x- and y-directions. Since the tool deflection is generally quite small compared to the tool dimensions, rotational displacements as a result of tool bending are neglected and, for the sake of simplicity, it is assumed that the tool is only displaced translationally as a result of the cutting forces. The substitute model for the shaper cutter thus consists of springs in the x- and y-directions, as shown in Fig. 7.

The displacement vector of the shaper cutter as a result of tool deflection can thus be calculated by

$$\begin{bmatrix} \Delta x_d \\ \Delta y_d \\ \Delta z_d \end{bmatrix} = \begin{bmatrix} k_x^{-1} & 0 & 0 \\ 0 & k_y^{-1} & 0 \\ 0 & 0 & 0 \end{bmatrix} \underline{F} \tag{31}$$

The transformation matrix $\underline{\underline{M}}_{2c_d}(t)$ to transform the shaper cutter from its own coordinate system S_c into the face-gear coordinate system S_2 taking the tool deflection into account is given by

$$\underline{\underline{M}}_{2c_d}(t) = \begin{bmatrix} \cos\phi_c \cos\phi_2 & -\sin\phi_c \cos\phi_2 & -\sin\phi_2 \sin\gamma & -(E+\Delta x_d)\cos\phi_2 \\ +\sin\phi_c \sin\phi_2 \cos\gamma & +\cos\phi_c \sin\phi_2 \cos\gamma & & \\ -\cos\phi_c \sin\phi_2 & \sin\phi_c \sin\phi_2 & -\cos\phi_2 \sin\gamma & (E+\Delta x_d)\sin\phi_2 \\ +\sin\phi_c \cos\phi_2 \cos\gamma & +\cos\phi_c \cos\phi_2 \cos\gamma & & \\ \sin\phi_c \sin\gamma & \cos\phi_c \sin\gamma & \cos\gamma & \dfrac{H_2 - d_r(t) + \Delta y_d}{\sin\gamma} \\ 0 & 0 & 0 & 1 \end{bmatrix} \tag{32}$$

with

$$\begin{aligned} \phi_c &= \phi_c(t) \\ \phi_2 &= \phi_2(t) \end{aligned} \tag{33}$$

It is thus obvious that the material removal per cutting stroke is also dependent on the tool deflection and therefore the material removal, the cutting forces and the tool deflection must be determined iteratively. For a cutting stroke, the uncut chip thicknesses without deflection are calculated first. Then the cutting forces are calculated and thus the tool deflection is determined. This results in new uncut chip thicknesses, cutting forces and tool deflections in the following iteration. The number of iterations required depends on how large the calculated tool deflections of two subsequent iterations may deviate from each other (abort criterion). In practice, the stiffness of the shaping machine tool is quite high, which means that the achieved tool deflection is very small compared

to the uncut chip thickness, which means that the deflection can be neglected when calculating the cutting forces. However, for shaping machine tools or clamping systems with low stiffness, tool deflection has a non-negligible influence on the cutting forces.

6. Tool wear

According to Usui et al. [22], the tool wear can be estimated by

$$\frac{dW}{\sigma_t\, dL} = C_1 \exp\left(-\frac{C_2}{T_{chip}[\mathrm{K}]}\right) \tag{34}$$

where dW is the material removal normal to the surface due to wear, σ_t is the normal stress, dL is the sliding distance, T_{chip} is the temperature of the chip surface in Kelvin and C_1 and C_2 are wear characteristic constants that depend on the cutting tool material and the material to be cut. For machining of 0.45C carbon steel with tungsten carbide P20 under classic cutting conditions and usual cutting speeds, Usui et al. [22] found the corresponding equation to estimate crater wear

$$\frac{dW}{\sigma_t\, v_c\, dt} = 0.01198\, \exp\left(-\frac{21'950}{T_{chip}[\mathrm{K}]}\right) \tag{35}$$

where v_c is the chip velocity and dt is a time increment. The equation to estimate flank wear is

$$\frac{dW}{\sigma_t\, v\, dt} = 7.8 \cdot 10^{-9}\, \exp\left(-\frac{5301.6}{T_{chip}[\mathrm{K}]}\right) \tag{36}$$

where v is the cutting speed. In order to estimate the temperature and the normal stress on the rake face, the model according to Moufki et al. [23] is applied. This model applies to the orthogonal cut, but is also used here for the oblique cut due to the small tool inclination angles. Moufki et al. [23] have chosen a distribution of the normal stress σ_t along the rake face as

$$\sigma_t(l) = \sigma_{t_0}\left(1 - \frac{l}{l_{ct}}\right)^{\xi_d} \tag{37}$$

where σ_{t_0} is the normal stress at the cutting edge acting orthogonally on the rake face, l_{ct} is the chip-tool contact length, l is the distance to the cutting edge and ξ_d is a profile parameter. Moufki et al. [23] have shown that a profile parameter of $\xi_d = 2$ represents the pressure profile well. According to Moufki et al. [23] the normal stress at the tool tip σ_{t_0} can be calculated by

$$\sigma_{t_0} = F_s \frac{\cos\beta_n}{\cos(\phi_{sn} + \beta_n - \gamma_n)} \cdot \frac{\xi_d + 1}{b\, l_{ct}} \tag{38}$$

where F_s is the shear force, β_n is the friction angle, ϕ_{sn} is the shear angle and γ_n is the rake angle. The equation for the tool-chip contact length l_{ct} is given by

$$l_{ct} = h\frac{\xi_d + 2}{2} \cdot \frac{\sin(\phi_{sn} + \beta_n - \gamma_n)}{\sin\phi_{sn}\cos\beta_n} \tag{39}$$

where h is the uncut chip thickness. According to Moufki et al. [23] the interface temperature along the rake face is calculated by

$$T_{chip}(l) = \frac{\bar{\mu}\,\sigma_{t_0}\sqrt{v_c}}{\sqrt{\pi\, k\, \rho\, c}}\left(l_{ct}^{-\xi_d}\sum_{i=0}^{\xi_d}\frac{2}{2i+1}C_{\xi_d}^{(i)}(l_{ct}-l)^{\xi_d - i}\, l^{\frac{2i+1}{2}}\right) + T_{chip_1}$$
$$\text{with } C_{\xi_d}^{(i)} = \frac{\xi_d!}{(\xi_d - 1)!\, i!} \tag{40}$$

where $\bar{\mu}$ is the mean friction coefficient, k is the thermal conductivity, ρ_m is the density and c is the specific heat capacity of the material to be cut. T_{chip_1} is the temperature at the outflow of the primary shear band and according to Moufki et al. [23] it is determined by

$$T_{chip_1} = T_w + \frac{\beta}{\rho\, c}\left(\rho(v\sin\phi_{sn})^2\frac{\gamma_1^2}{2} + \tau_0\,\gamma_1\right) \tag{41}$$

where T_w is the absolute temperature of the work-piece, β_{TQ} is the Taylor–Quinney coefficient, γ_1 is the shear strain at the outflow of the primary shear band and τ_0 is the shear stress at the entry of the band. The shear strain at the outflow of the primary shear band γ_1 is calculated by

$$\gamma_1 = \tan(\phi_{sn} - \gamma_n) + \frac{1}{\tan\phi_{sn}} \tag{42}$$

In order to estimate the shear stress τ_0 at the entry of the band a simplification is made compared to the approach by Moufki et al. [23]: The shear stress τ_0 is determined by

$$\tau_0 = \tau_1 - \rho(v\sin\phi_{sn})^2\gamma_1 \tag{43}$$

with

$$\tau_1 = \frac{F_s\sin\phi_{sn}}{b\, h} \tag{44}$$

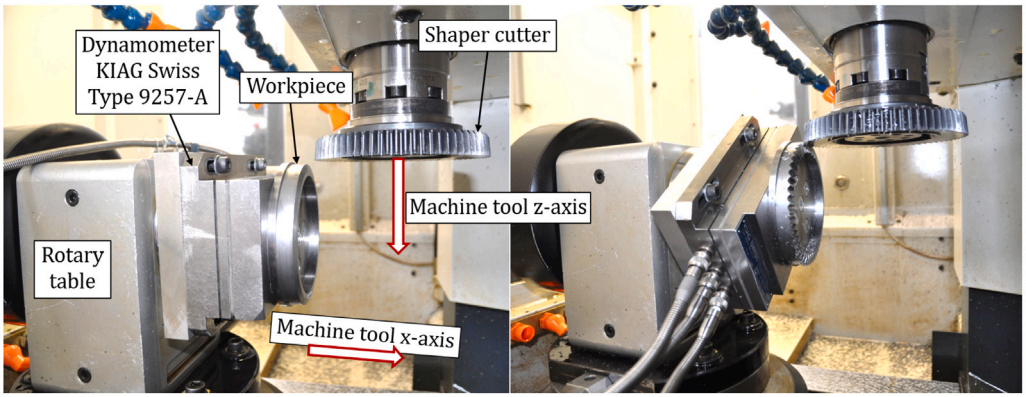

Fig. 8. Gear shaping measurement setup. Left: Setup before experiment; Right: Setup after experiment.

The mean friction coefficient $\bar{\mu}$ depends on the temperature as well. For this, Moufki et al. [23] use the dependency of the mean friction coefficient $\bar{\mu}$ on a mean temperature $\bar{T}_{chip}$. They found following empirical equations for steel on steel friction

$$\bar{\mu} = \begin{cases} 1 - 3.44 \cdot 10^{-4}\, \bar{T}_{chip}, & 25\ °\text{C} \le \bar{T}_{chip} \le 955\ °\text{C} \\ 0.68\left(1 - \dfrac{\bar{T}_{chip} - T^*}{T_m - T^*}\right)^q, & 955\ °\text{C} \le \bar{T}_{chip} \le 1500\ °\text{C} \end{cases} \tag{45}$$

with $T^* = 955\ °\text{C}$, $T_m = 1500\ °\text{C}$, $q = 1.7$

The mean temperature $\bar{T}_{chip}$ is calculated by

$$\bar{T}_{chip} = \frac{\bar{\mu}\,\sigma_{t_0}\sqrt{v_c\, l_{ct}}}{\sqrt{\pi\, k\, \rho\, c}} \sum_{i=0}^{\xi_d} \frac{2}{2i+1} C_{\xi_d}^{(i)} \left(\sum_{j=0}^{\xi_d - 1} (-1)^j C_{\xi_d - 1}^{(j)} \frac{2}{2(i+j)+3} \right) + T_{chip_1} \tag{46}$$

It is therefore obvious that the coefficient of friction and the temperature are interdependent. The two equations are solved numerically. The following equation can be used as a starting value for the mean coefficient of friction

$$\bar{\mu} = \tan \beta_n \tag{47}$$

The crater wear can be estimated with the normal stress and temperature curves determined in this way. For the flank wear, the normal stress and temperature at the tool tip are used in a simplified manner. Unfortunately, it turns out that unrealistic values are determined for small chip thicknesses. On the one hand, the Kienzle equation is only correct to a limited extent for very small chip thicknesses, unless tests were carried out directly with small chip thicknesses. On the other hand, the temperatures are significantly overestimated. However, it has been shown that plausible values are calculated from an uncut chip thickness of approximately $h = 25\ \mu\text{m}$. For this reason, uncut chip thicknesses smaller than $h = 25\ \mu\text{m}$ are not taken into account when calculating the wear. It is clear that an exact prediction with regard to the wear is not possible, however, a qualitative assessment of various machining parameters with regard to the wear should be feasible.

7. Experimental validation

In order to validate the gear shaping simulation, the cutting forces for an example face-gear made of 20MnCr5 (1.7147) were measured and compared with the simulated forces. The Kienzle parameters were taken from the table book of Apprich et al. [24]. The machining took place on a Lorenz gear shaping machine tool, which was equipped with an additional rotary table as A-axis for the production of face-gears. Due to the limited installation space, the outer diameter of the face-gear is the maximum possible value of $d_{a2} = 120\ \text{mm}$, with the shaper cutter having a significantly higher number of teeth than the face-gear. This made it possible to install a dynamometer between the rotary table and the workpiece without the device colliding with the spindle. The dynamometer used is the 9257-A from KIAG Swiss. Fig. 8 shows the measurement setup.

The shaper cutter is made of high speed steel and has a tip rake angle of $\gamma_{sc} = 5°$ (Table 1). Since the rake face of the shaper cutter is conical, the effective rake angle changes along the cutting edge in such a way that it corresponds to the tip rake angle at the tooth addendum, but the effective rake angle drops until 0° starting from the addendum along the flanks. At the flanks, the tip rake angle thus practically acts as the inclination angle. The tip clearance angle of the shaper cutter is $\alpha_{sc} = 6°$ (Table 1). The effective clearance angle is also not constant over the cutting edge. Starting from the tool addendum, the effective clearance angle decreases along the flank.

Table 1
Design parameters and main data of the test face-gear for manufacturing by gear shaping.

Design parameter/component	Symbol	Unit	Value
Shaper cutter			
Number of teeth	N_{sc}	—	68
Normal module	m_n	mm	2
Normal pressure angle	α_n	°	20
Tip rake angle	γ_{sc}	°	5
Tip clearance angle	α_{sc}	°	6
Helix angle	β	°	0
Material	HSS coated		
Face-gear			
Number of teeth	N_2	—	48
Shaft angle	γ_s	°	90
Axle offset	E	mm	0
Inner diameter	D_{i2}	mm	100
Outer diameter	D_{a2}	mm	120
Material	20MnCr5 (1.7147)		
Kienzle parameter [24]			
Specific cutting force	$k_{c1,1}$	$\mathrm{N\,mm^{-2}}$	2140
Cutting exponent	m_c	—	0.25
Specific feed force	$k_{f1,1}$	$\mathrm{N\,mm^{-2}}$	340
Feed exponent	m_f	—	0.68
Gear shaping parameter			
Cutting stroke frequency	f_{st}	$\mathrm{min^{-1}}$	428
Radial start infeed	$a_{r_{start}}$	mm	0.003
Radial end infeed	$a_{r_{end}}$	mm	0.003
Circumferential infeed	a_{circ}	mm	0.1
Stroke length	l_{st}	mm	23.8
Top overrun length	l_{top}	mm	3

In order to avoid a collision of the dynamometer with the rotary table of the C-axis, a face-gear segment of approximately 220° was manufactured. This segment includes the complete radial immersion of the cutter as well as an area in which only the circumferential feed is active. After the tool is completely immersed in the radial direction, the cutting forces show a practically recurring pattern until the starting angle of the face-gear is reached. Thus, even when processing a larger segment, no additional gain in knowledge would be expected. A representative comparison of the measurements with the simulation is thus given with the given face-gear segment. Table 1 lists the data of the shaper cutter and face-gear as well as the selected process data.

The correction factor K_γ to account for the influence of the rake angle on the cutting forces, the equation according to Andrich et al. [24] is used

$$K_\gamma = 1 - \frac{\gamma - \gamma_0}{100°} \tag{48}$$

where γ_0 is the basic rake angle. For steel it is set to $\gamma_0 = 6°$. The correction factor for chip compression is set to $K_{sp} = 1.1$ for gear shaping according to Andrich et al. [24]. The influence of the cutting speed on the cutting forces is approximately taken into account by the correction factor K_{v_c}, calculated by

$$K_{v_c} = \left(\frac{100}{v}\right)^{0.1}, v\,[\mathrm{m\,s^{-1}}] \tag{49}$$

The correction factor K_{wear}, which takes into account the influence of tool wear, is set to $K_{wear} = 1$, since an unworn tool was used. Due to the short duration of the test and the fact that the tool does not make a full revolution during the test, no influence due to tool wear is expected for the experiment. From this, for the overall cutting force correction factor it follows

$$K_c = K_f = K_\gamma\, K_{sp}\, K_v\, K_{wear} \tag{50}$$

Fig. 9 shows the measured cutting force and the values determined by simulation in x-direction, Fig. 10 shows the result in y-direction and Fig. 11 shows the corresponding result in z-direction. The results are given for the machine tool coordinate system, where the z-direction corresponds to the stroke direction of the shaper cutter.

Qualitatively, there is good match between the simulation results and the measured values. The increased machining forces when plunging the tool are clearly recognizable and run analogously for the simulation as well as the measurement. In particular, the cutting force in the z-direction shows good quantitative agreement. The force in the x-direction also shows good quantitative agreement, while the measured force in the y-direction corresponds to only about 50% of the calculated force. The dominant force is the one in cutting direction, which is well reproduced by the simulation. Although the force component in the y-direction is quite small compared to the force in the cutting direction, the discrepancy between simulation and measurement is still relatively large, especially considering the good agreements for the other two directions. Here, further research and experiments, with other tool and

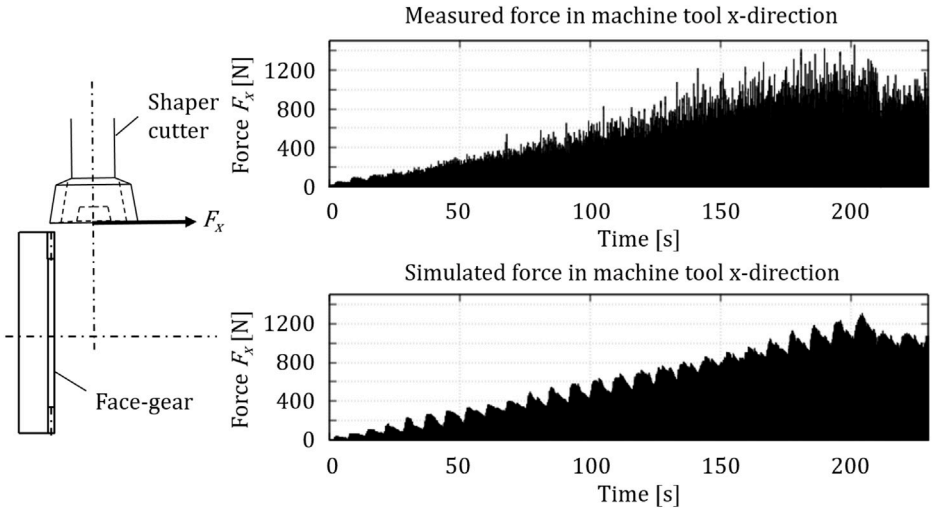

Fig. 9. Measured and simulated cutting force during gear shaping in the x-direction of the machine tool.

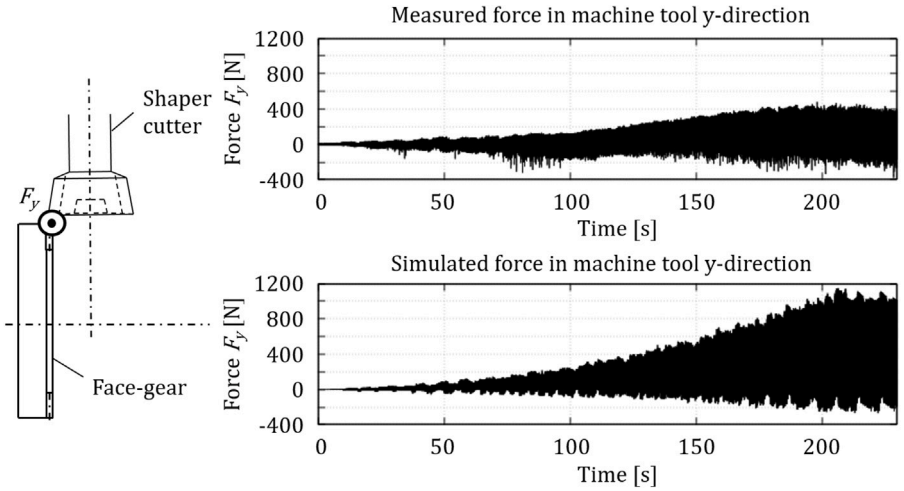

Fig. 10. Measured and simulated cutting force during gear shaping in the y-direction of the machine tool.

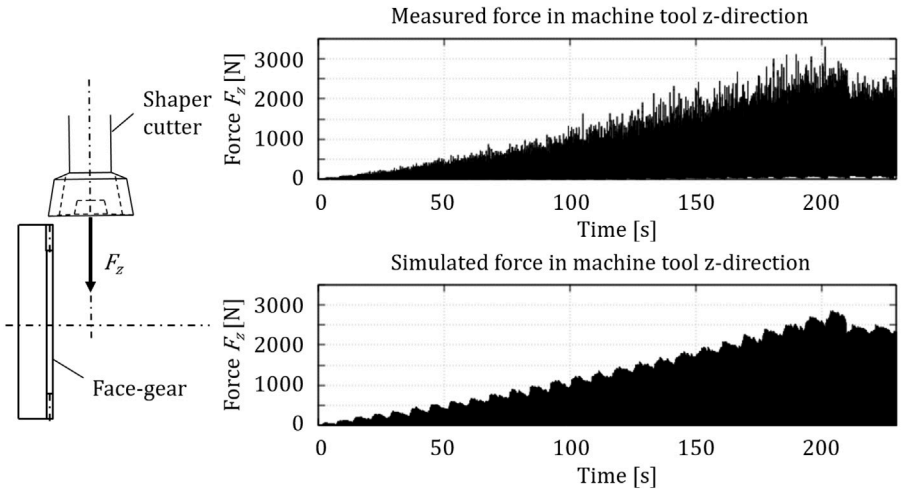

Fig. 11. Measured and simulated cutting force during gear shaping in the z-direction of the machine tool.

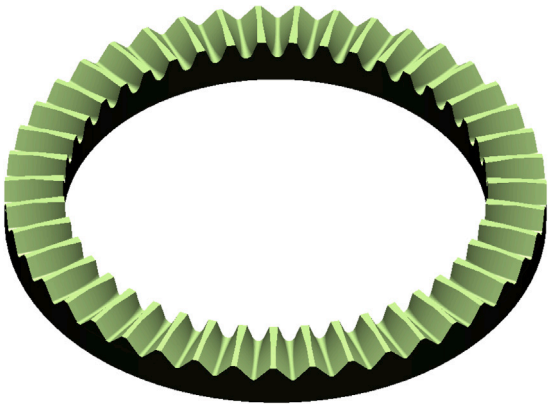

Fig. 12. Test face-gear for manufacturing on a 5-axis machine tool.

face-gear geometries and also different materials, would be desirable in the future. It is also noticeable that some force peaks can be found in the measurements, which indicates additional dynamic effects that are not considered in the simulation. It should also be noted that the chip thicknesses are by no means constant over the stroke length, but the parameters from the Kienzle equation were determined for constant chip thicknesses. Overall, a good agreement between simulation and measurement can be observed despite the assumptions made.

It should also be mentioned that the calculated force in the z-direction is almost completely determined by the Kienzle parameters in the cutting direction, while the parameters in the feed direction are decisive for the forces in the x- and y-direction. Usually, when determining the Kienzle parameters, the focus is on the forces in the cutting direction, so that for less investigated materials often only little information on the forces in the feed direction can be found in the literature. In the future, it could be a problem to obtain the correct Kienzle parameters from the literature for some materials, especially if hardened or nitrided materials are used. Here, an indirect parameter determination could be useful: First, the cutting forces during the machining of a face-gear must be measured, then the simulations are carried out for the same geometry, whereby the Kienzle parameters are iteratively adjusted until the calculated forces match the measured values.

8. Application of the gear shaping simulation

In the following, the application of the gear shaping simulation will be explained. The face-gear with the design parameters according to Table 2 made of C45 steel serves as an example. Fig. 12 shows the face-gear. It is a straight-toothed face-gear without axle offset with 43 teeth. The shaper cutter is made of solid tungsten carbide and has a tip rake angle of $\gamma_{sc} = 5°$ (Table 2). Martinovs et al. [25] built formulae for the specific heat capacity c and the thermal conductivity k of C45 steel. The formula for the specific heat capacity c is given by

$$c = 50 + 450 \cdot \exp\left[-\left(\frac{T - 980}{50}\right)\right] + 20T^{0.53} - 0.0021T^{1.66} \tag{51}$$

and the formula for the thermal conductivity k is given by

$$k = 2 \cdot 10^{-8}T^3 - 4 \cdot 10^{-5}T^2 - 0.0045T + 54 \tag{52}$$

where T is the metal temperature. For the chip temperature calculations, however, the mean temperature $\bar{T}_{chip}$ is used. Both equations were determined by approximating experimental data provided by Lazić et al. [26].

The characteristic values of the Kienzle equation were taken from the book of tables by Apprich et al. [24]. The Taylor–Quinney coefficient was assumed to be $\beta_{TQ} = 1$. The relevant data are summarized in Table 2.

The cutting stroke frequency is chosen as $f_{st} = 400\,\mathrm{min}^{-1}$ and the stroke length l_{st} is selected according to the tooth width, or is based on the specifications of the shaping machine tool. The initial circumferential infeed $a_{circ} = 0.25$ mm is estimated considering a certain maximum uncut chip thickness and requirements regarding maximum allowed deviations in the flank surface topography. An initial radial infeed of $a_r = 0.05$ mm is selected. In order to be able to estimate the tool deflection as an example, a stiffness of the system consisting of workpiece, clamping system, tool and machine tool of $k_x = k_y = 10^7\,\mathrm{N\,m}^{-1}$ is assumed. Fig. 13 shows the resulting cutting forces for these initial parameters in the coordinate system of the gear shaping machine tool as shown in Fig. 8. In this particular configuration, the force in the y-direction corresponds to the cutting force, i.e. it is the direction of the double stroke movement. The z-direction corresponds to the direction of the radial infeed and the x-direction is orthogonal to the other two directions. At around $t = 13\,\mathrm{s}$ there is a peak force, which indicates that the radial infeed a_r is chosen too high.

In the following, the radial feed is to be optimized in such a way that the radial infeed takes place as quickly as possible, but there shall be no increase in the machining forces and the tool life shall not be adversely affected. For this purpose, the mean radial

Table 2
Design parameters and main data of the test face-gear for manufacturing by gear shaping.

Design parameter/component	Symbol	Unit	Value
Shaper cutter			
Number of teeth	N_{sc}	—	14
Normal module	m_n	mm	2.2
Normal pressure angle	α_n	°	20
Tip rake angle	γ_{sc}	°	5
Profile shift coefficient	x_{sc}	—	0.4931
Helix angle	β	°	0
Material	Tungsten carbide		
Face-gear			
Face-gear number of teeth	N_2	—	43
Shaft angle	γ_s	°	90
Axle offset	E	mm	0
Face-gear inner diameter	D_{i2}	mm	94.6
Face-gear outer diameter	D_{a2}	mm	120.8
Material	C45 (1.0503)		
Density	ρ	kg m^{-3}	7800
Kienzle parameter, Usui constants			
Specific cutting force	$k_{c1,1}$	N mm^{-2}	1680
Cutting exponent	m_c	—	0.26
Specific feed force	$k_{f1,1}$	N mm^{-2}	340
Feed exponent	m_f	—	0.68
C_1	0.01198 (crater wear), $7.8 \cdot 10^{-9}$ (flank wear)		
C_2	21'950 (crater wear), 5301.6 (flank wear)		

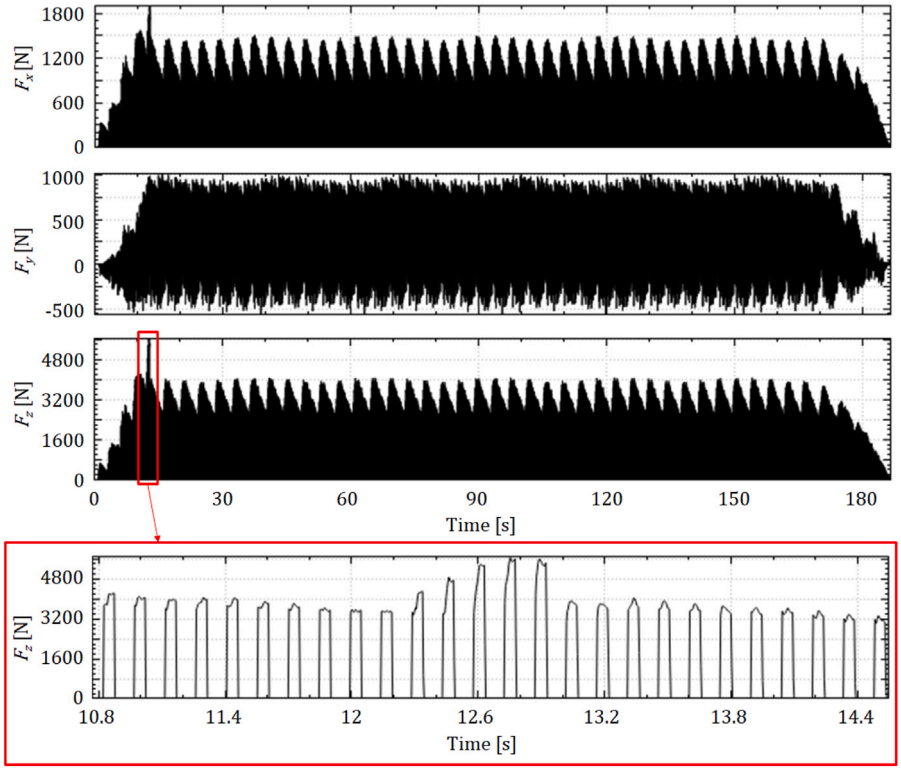

Fig. 13. Simulated cutting forces for shaping the face-gear with the initially chosen infeeds. At a time of approximately $t = 13$ s there is an increased force, which indicates that the radial infeed a_r is too high. $f_{sI} = 400\,\text{min}^{-1}$, $a_r = a_{r_{start}} = a_{r_{end}} = 0.05$ mm, $a_{circ} = 0.25$ mm.

infeed a_r is now varied, as well as the distribution between the start infeed $a_{r_{start}}$ and the end infeed $a_{r_{end}}$. Since the radial feed is a uniformly accelerated movement, the manufacturing time also remains constant with a constant mean infeed. Fig. 14 shows how the cutting forces, tool wear and the maximum uncut chip thickness behave depending on the radial infeed. The maximum uncut

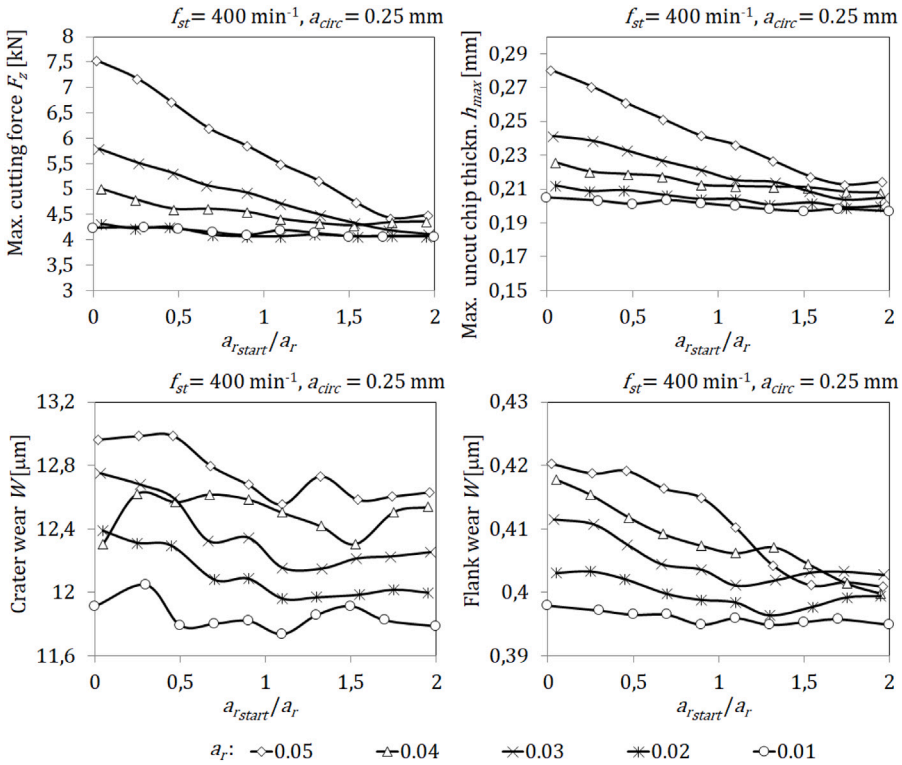

Fig. 14. Simulated results for shaping the face-gear with a cutting stroke frequency of $f_{st} = 400\,\mathrm{min}^{-1}$, constant circumferential infeed $a_{circ} = 0.25$ mm and varied radial infeed a_r. Top left: Maximum cutting force F_z; Top right: Maximum uncut chip thickness h_{max}; Bottom left: Crater wear calculated according to Eq. (35); Bottom right: Flank wear calculated according to Eq. (36). $a_r = 0.5(a_{r_{start}} + a_{r_{end}})$.

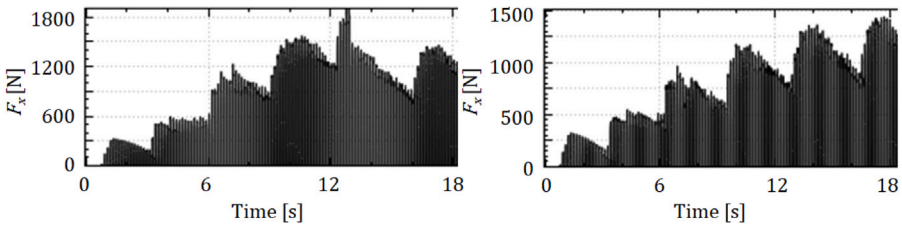

Fig. 15. Cutting forces F_x during radial infeed. $f_{st} = 400\,\mathrm{min}^{-1}$, $a_{circ} = 0.25$ mm. Left: $a_{r_{start}} = a_{r_{end}} = 0.05$ mm, Right: $a_{r_{start}} = 0.05$ mm, $a_{r_{end}} = 0$ mm.

chip thickness is the uncut chip thickness that has occurred over the entire machining process and along the active cutting edge. This is important insofar as the forces alone do not allow any statement about a local overload of the tool. Pure optimization after the flank or crater wear must also be used with caution, since it cannot determine overloading of the cutting edge: The problem is that large chip thicknesses occurring for a short time can lead to cutting edge chipping while the calculated wear is still small. It can be seen that with maximum radial infeed at the start and a reduction in the radial infeed over the immersion depth, the machining forces and the maximum chip thickness decrease. The same applies to tool wear, but the differences are so small that the calculated wear is not a suitable evaluation criterion. The optimum radial feed rates are therefore found if, with a further reduction in the feed rates, there is no reduction in the cutting forces and no reduction in the maximum chip thickness. In this example, this point is reached with a radial start infeed of $a_{r_{start}} = 0.04$ mm and an end infeed of $a_{r_{end}} = 0$ mm.

Further calculations have shown that the radial start infeed can even be increased to $a_{r_{start}} = 0.05$ mm without increasing the cutting forces and the maximum uncut chip thickness. Fig. 15 shows the cutting forces F_x during radial infeed for the initial infeeds as well as the forces for the optimized infeeds.

A further reduction of the radial infeed does not bring any advantages in terms of cutting forces, uncut chip thicknesses and tool wear, but increases the machining time. The processing time depending on the radial infeed is shown in Fig. 16. It is obvious that as the mean radial infeed becomes smaller, the production times increase drastically and thus the profitability decreases. This is another reason why finding suitable values for the start and end infeeds is of particular interest.

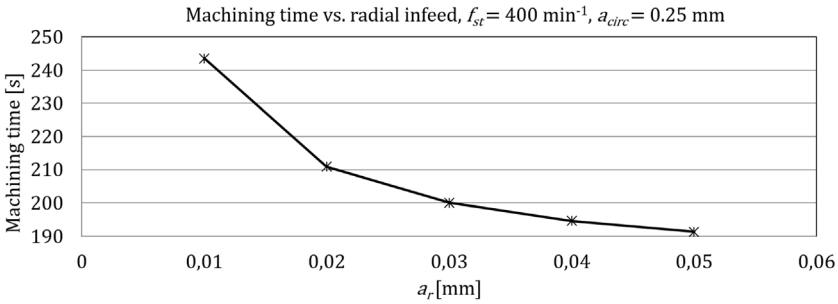

Fig. 16. Machining time over the mean radial infeed. $f_{st} = 400\,\mathrm{min}^{-1}$, $a_{circ} = 0.25$ mm.

Table 3
Design parameters and main data of test face-gear for manufacturing by gear shaping.

Parameter	Symbol	Unit	Strategy 1	Strategy 2
Radial start infeed	$a_{r_{start}}$	mm	0.033	0.0026
Radial end infeed	$a_{r_{end}}$	mm	0	0.0014
Circumferential infeed	a_{circ}	mm	0.158	0.25
Maximum cutting force	F_z	N	3009	3045
Maximum uncut chip thickness	h_{max}	mm	0.128	0.176
Crater wear	W	µ m	18.43	17.14
Flank wear	W	µ m	0.57	0.53
Machining time	t	s	322	504

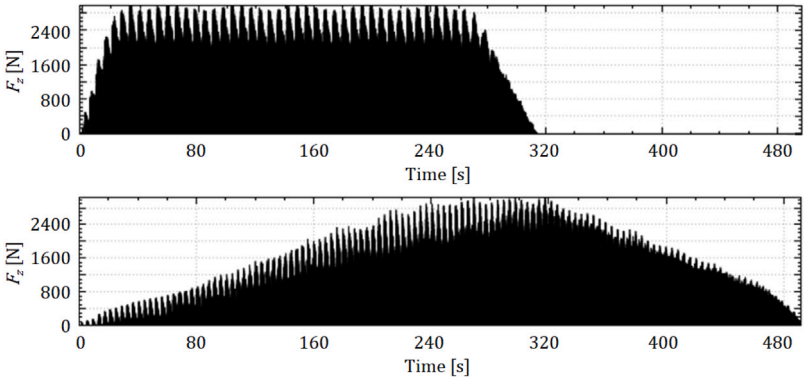

Fig. 17. Resulting cutting forces F_z for the both strategies chosen to reduce the maximum cutting force. Top: Reduced circumferential infeed a_{circ}. Bottom: Reduced radial infeed a_r.

In the following, for example, the cutting forces should be reduced to a maximum of $F_z = 3\,\mathrm{kN}$. For this purpose, two strategies will now be compared: One strategy is the reduction of the circumferential infeed a_{circ} while at the same time optimizing the radial infeed, as just presented. The second strategy is to keep the circumferential infeed at $a_{circ} = 0.25$ mm and to immerse the tool very slowly in radial direction and to optimize the distribution of the radial infeed at start and end according to the crater wear. In Table 3, the results for both strategies are listed. The cutting forces are shown in Fig. 17. It can be clearly seen that the machining time with the reduced radial infeed is significantly higher with strategy 2. The maximum uncut chip thickness is also significantly increased for strategy 2. In any case, the slightly lower tool wear cannot justify the significantly higher machining time. The problem with the reduced radial infeed consists in the fact that, on average, the material removal per time is smaller, but the tip of the shaper cutter teeth mainly contributes to the material removal. This means that tool wear is also concentrated on the tip of the shaper cutter teeth. The crater wear for both strategies is shown in Fig. 18.

Fig. 19 shows an example of the pressure and temperature distribution along the cutting edge for a specific time point. These distributions always change over the stroke movement, just as the area of the cutting edge in engagement shifts over time. The pressure acting on the rake face decreases steadily from the cutting edge over the rake face. The highest temperatures, however, are not reached on the cutting edge itself but on the rake face further inside, which causes the typical crater wear.

The common practice of choosing the radial infeed as large as possible is also confirmed when shaping face-gears, because with this strategy the material removal is better distributed along the cutting edge. The tip area of the individual teeth of the shaper cutter mainly contributes to the material removal in general and is therefore more affected by wear. Small radial infeeds lead to an even bigger wear concentration at the tooth tips.

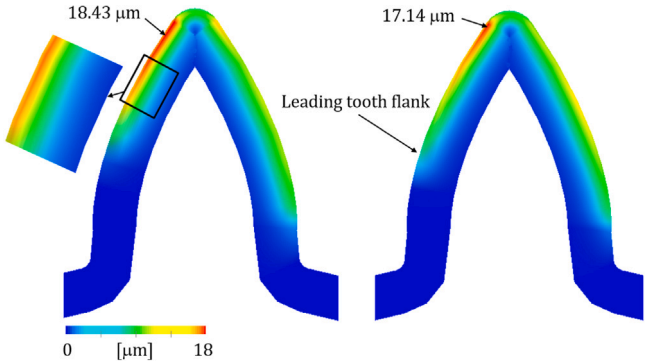

Fig. 18. Crater wear of the two strategies. Left: Strategy 1, reduced circumferential infeed a_{circ}, Right: Strategy 2, reduced radial infeed a_r.

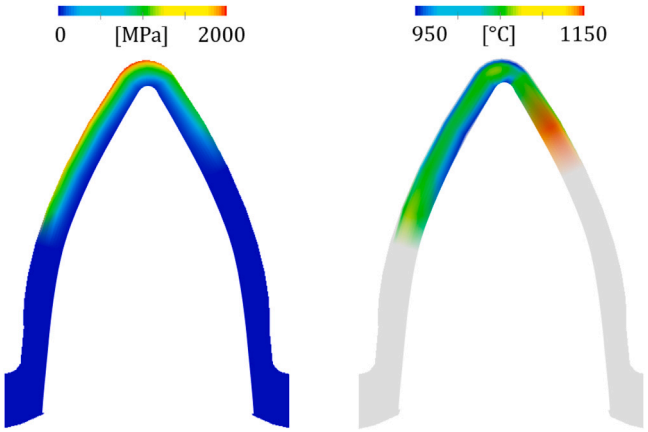

Fig. 19. Example of the pressure and temperature distribution along the cutting edge for a specific time point. Left: Pressure distribution along cutting edge, Right: Temperature distribution along cutting edge.

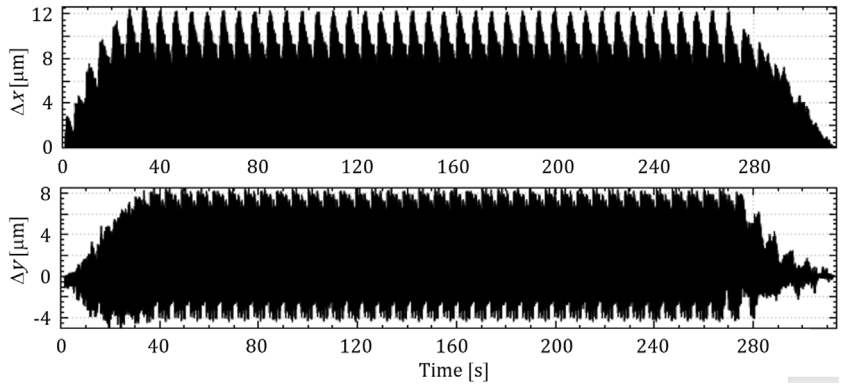

Fig. 20. Tool Deflection for strategy 1 in x- and y-direction of the machine tool coordinate system according to Fig. 8.

For strategy 1, the tool deflection over time for the assumed stiffness in x- and y-direction of $k_x = k_y = 10^8 \mathrm{N\,m^{-1}}$ is shown in Fig. 20. If the system of machine tool, workpiece clamping and tool is stiff enough, the corresponding tool deflection is low. If the corresponding deflections become too large, a reduction of the radial and/or circumferential infeed shall be considered, at least for the finishing cut. It should be noted that the deflection shown is only an estimate, as dynamic effects are neglected. Katz et al. [10] present an approach on how the dynamic behaviour when gear shaping cylindrical gears can be taken into account. The application of this approach to the gear shaping of a face-gear could be the subject of future research.

Using the simulation of the shaping process, cutting forces, uncut chip thicknesses and tool wear can efficiently be estimated. In this way, the process parameters, such as the individual infeeds, can be optimized. Optimization through experimental trials, on the

other hand, is difficult. The problem is that some parameters, such as the uncut chip thickness, cannot be measured. Furthermore, a measured force does not allow any conclusions to be drawn about the local stress along the cutting edge. The simulation enables a deeper insight into the processes involved in gear shaping and thus helps to select infeeds in such a way that short machining times are achieved in combination with a long tool lifetime.

9. Conclusions

Gear shaping is a complex manufacturing process. Depending on the infeeds selected, the uncut chip thicknesses change considerably, as do the areas of the cutting edge that are involved in the material removal. Finding suitable machining parameters is very much dependent on experience and multiple test gears are necessary before the manufacturing process runs satisfactorily.

The simulation of gear shaping has considerable advantages. Uncut chip thicknesses can be determined in advance and suitable infeeds can be found in the direction of the tooth height, so that the fastest possible immersion is possible without increasing the machining forces. Different feed strategies can be compared with each other, also taking tool wear into account. The resulting optimization possibilities are very diverse: Depending on the requirements, e.g. tool life, machining time or their combinations can be improved. The number of test gears for finding suitable parameters and the number of reject gears can thus be reduced. Above all, many more parameter data sets can be tested through simulation, which would be very expensive and time consuming in practice and therefore quickly uneconomical.

At the moment, the assessment of tool wear is viewed more critically. The areas with the highest wear fit very well with practice and conclusions can also be drawn with regard to different parameter data sets, but proof of the quantitative correctness has yet to be provided. There is enough potential for future research in this area in particular. In addition, gear shaping simulation offers the potential to determine Kienzle parameters in an indirect way by measuring the cutting forces on the machine tool for the shaping of a face-gear and adjusting the Kienzle parameters until the simulation result matches the measurement.

Declaration of competing interest

The authors declare that they have no known competing financial interests or personal relationships that could have appeared to influence the work reported in this paper.

Acknowledgements

Funding: This work was supported by Innosuisse, the Swiss Innovation Agency, Switzerland [project no. 36294.1 INNO-ENG]. The authors would like to thank Daniel Arn, Ueli Ruch and Vule Spasic from the industrial partner Hans Christen AG for making the gear shaping experiment possible.

References

[1] Edward W. Miller, Hob for generating crown gears, Google Patents. US Patent 2,304,586, 1942.
[2] B.V. Crown Gear, Tools for manufacturing crown wheels, and method for manufacturing such tools, Google Patents. Patent NL9002611A, 1992.
[3] B.V. Crown Gear, Tools for manufacturing crown wheels, Google Patents. Patent NL9300226A, 1994.
[4] B.V. Crown Gear, Tools for manufacturing a crown wheel that can cooperate with a bevel tooth pinion and method of manufacturing such a crown wheel, Google Patents. Patent NL9300826A, 1994.
[5] Yan-Zhong Wang, Liang-Wei Hou, Zhou Lan, Can-Hui Wu, Qing-Jun Lv, Xing-Fu Zhao, A precision generating hobbing method for face-gear based on worm hob, Proc. Inst. Mech. Eng. Part C. J. Mech. Eng. Sci. 231 (6) (2017) 1057–1071.
[6] Yan-Zhong Wang, Xiao-Meng Chu, Wen-Jun Zhao, Zhuo Wang, Guo-Ying Su, Yi-Zhan Huang, A precision generating hobbing method for face gear with assembly spherical hob, J. Central South Univ. 26 (10) (2019) 2704–2716.
[7] Yunbo Shen, Jinglin Tong, Technology of gear shaping of face gear and experimental studies, in: 2010 International Conference on Digital Manufacturing & Automation, vol. 2, IEEE, 2010, pp. 609–612.
[8] Kaan Erkorkmaz, Andrew Katz, Yasin Hosseinkhani, Denys Plakhotnik, Marc Stautner, Fathy Ismail, Chip geometry and cutting forces in gear shaping, CIRP Ann. 65 (1) (2016) 133–136.
[9] Andrew Katz, Kaan Erkorkmaz, Fathy Ismail, Virtual model of gear shaping—part i: Kinematics, cutter–workpiece engagement, and cutting forces, J. Manuf. Sci. Eng. 140 (7) (2018).
[10] Andrew Katz, Kaan Erkorkmaz, Fathy Ismail, Virtual model of gear shaping—part ii: Elastic deformations and virtual gear metrology, J. Manuf. Sci. Eng. 140 (7) (2018).
[11] Andrew Katz, Cutting mechanics of the gear shaping process, (Master's thesis), University of Waterloo, 2017.
[12] Man Xu, Xinghui Han, Lin Hua, Fangyan Zheng, Modeling and methods for gear shaping process and cutting force prediction of variable transmission ratio rack, Int. J. Mech. Sci. 171 (2020) 105364.
[13] Otto Kienzle, Die bestimmung von kräften und Leistungen an spanenden Werkzeugen und Werkzeugmaschinen, VDI-Z 94 (11) (1952) 299–305.
[14] Zeki Yazar, Karl-Friedrich Koch, Tom Merrick, Taylan Altan, Feed rate optimization based on cutting force calculations in 3-axis milling of dies and molds with sculptured surfaces, Int. J. Mach. Tools Manuf. 34 (3) (1994) 365–377.
[15] Wilfried A. König, Klaus Essel, Lothar Witte, Specific cutting force data for metal-cutting, Verlag Stahleisen, 1982.
[16] E. Budak, Y. Altintas, EJA Armarego, Prediction of milling force coefficients from orthogonal cutting data, 1996.
[17] Y. Altintas, Modeling approaches and software for predicting the performance of milling operations at MAL-UBC, Mach. Sci. Technol. 4 (3) (2000) 445–478.
[18] M. Kaymakci, Z.M. Kilic, Y. Altintas, Unified cutting force model for turning, boring, drilling and milling operations, Int. J. Mach. Tools Manuf. 54 (2012) 34–45.
[19] E.H. Lee, The theory of plasticity applied to a problem of machining, ASME J. Appl. Mech. 18 (1951) 405.
[20] A.M. Kovrizhnykh, Determining the shear angle, forces, and sizes of shearing elements during metal cutting, J. Appl. Mech. Tech. Phys. 50 (1) (2009) 147–154.

[21] EJA Armarego, The unified-generalized mechanics of cutting approach—a step towards a house of predictive performance models for machining operations, Mach. Sci. Technol. 4 (3) (2000) 319–362.
[22] E. Usui, T. Shirakashi, T. Kitagawa, Analytical prediction of cutting tool wear, Wear 100 (1-3) (1984) 129–151.
[23] A. Moufki, Alain Molinari, D. Dudzinski, Modelling of orthogonal cutting with a temperature dependent friction law, J. Mech. Phys. Solids 46 (10) (1998) 2103–2138.
[24] Thomas Apprich, Josef Brenner, Michael Dambacher, Franz Dreher, Georg Fischer, Gerd Greiner, Burkhard Heine, Armin Hochstatter, Sven Holzberger, Fabian Holzwarth, et al., Tabellenbuch für Zerspantechnik, Verlag Europa-Lehrmittel Nourney, Vollmer GmbH & Company KG, 2016.
[25] Andris Martinovs, Svetlana Polukoshko, Edgars Zaicevs, Ritvars Revalds, Laser hardening process optimization using FEM, Eengineering Rural Dev. (2020) 1500–1508.
[26] Vukić N. Lazić, Ivana B. Ivanović, Aleksandar S Sedmak, Rebeka Rudolf, Mirjana M Lazić, Zoran J Radaković, Numerical analysis of temperature field during hardfacing process and comparison with experimental results, Therm. Sci. 18 (suppl. 1) (2014) 113–120.